Theor. Appl. Climatol. 54, 235–248 (1996)

Theoretical and Applied Climatology

Canada Centre for Remote Sensing, Ottawa, Ontario, Canada

On the Angular Correction of Satellite Radiation Measurements: The Performance of ERBE Angular Dependence Model in the Arctic

Z. Li

With 6 Figures

Received January 30, 1995
Revised June 15, 1995

Summary

An angular dependence model (ADM) is needed to convert radiance measurements into fluxes. This paper provides an overview on the progress and issues related to the angular correction of radiation data at the top-of-the-atmosphere (TOA), followed by an investigation on the performance of the Earth Radiation Budget Experiment (ERBE) ADMs in the Arctic during summer. The variation of inferred albedo with viewing geometry indicates the merit of an ADM. The ERBE ADM for land does well as it leads to near constant albedos for given solar zenith angles. The ADM for snow/ice is least satisfactory when applied to the Arctic in summer. The performance of the ocean ADM is acceptable except at large solar zenith angles for which albedo increases with viewing zenith angle. Significant and systematic variation of albedo with viewing angle and relative azimuth angle are manifest when the overcast ERBE ADM is applied to overcast-over- snow/ice scenes. A methodology for correcting ERBE ADMs was proposed by normalizing the anisotropic factor over bins containing sufficient measurements.

1. Introduction

The Earth Radiation Budget Experiment (ERBE) (Barkstrom and Smith, 1986) is one of the most successful space programs ever launched. It has been demonstrated to be a unique data base for addressing some critical issues concerning the Earth's climate. By analyzing ERBE data, it was revealed that clouds have an overall radiative cooling effect on the planet, while regional and seasonal effects may be warming or cooling (Ramanathan et al., 1989; Harrison et al., 1990; Arking, 1991). As a result, ERBE data have been widely used for diagnostic studies of general circulation models (Kiehl and Ramanathan, 1990; Cess et al., 1992; Barker et al., 1994). Although ERBE provides only the top-of-the-atmosphere (TOA) radiation measurements, the TOA shortwave data have been used to estimate surface solar radiation budget (Li and Leighton, 1993) with promising accuracy (Li et al., 1995). With the capability for provision of reliable data on the radiation budgets at both the TOA and the surface, ERBE has become more appealing to the diagnostic studies of climate modelling (Barker and Li, 1995).

Despite the successes of ERBE, one must bear in mind that the radiative flux data provided by ERBE are not direct measurements. In fact, numerous inversion algorithms were employed during data processing including calibration, scene identification, spectral and angular corrections, spatial and temporal averaging, etc. (Smith et al., 1986). Although meticulous considerations were paid for in the design of each algorithm, the quality of instantaneous ERBE data is not well defined. The most uncertain step lies in the angular correction that converts radiance observations

to fluxes using angular dependence models (ADMs) (Stuhlmann and Raschke, 1987). Uncertainties due to the ERBE angular correction may lead to an absolute error of nearly 2% in the global mean albedo (Ye, 1993). To date, the performance of ERBE ADMs has been investigated mainly over oceans at low latitudes that were viewed by the Earth Radiation Budget Satellite (ERBS). For example, Baldwin and Coakley (1991) estimated the uncertainty due to incorrect bidirectional correction for oceans of various cloud covers and found that maximum bias and random errors are 4% and 15%, respectively. Dlhopolsky and Cess (1993) illustrated that the anisotropy of reflected radiation over clear oceans is severely undertreated by ERBE in the forward scattering direction. Suttles et al. (1992) found that TOA albedo derived by applying ERBE ADMs to NIMBUS-7 earth radiation budget (ERB) scanner data has a systematic dependence on viewing zenith angle; a variation of 0.1 from near nadir to near limb. Note that ERBE ADMs were actually constructed using primarily NIMBUS-7 ERB data (Suttles et al., 1988).

In view of potential problems with ERBE angular correction, this study examines the performance of the ERBE ADM in the Arctic during summer. In addition to the importance of studying polar radiation budgets, selection of this particular area stems from technical considerations. First, the convergence of polar orbits in the Arctic and the ERBE cross-track scanners permit multiple observations from various viewing geometries with high repetitive frequency. This is a basic requirement for an ADM study, when simultaneous observations from different viewing angles are unavailable. Second, various geographic types (geotype) co-exist in the Arctic during summer such as open water, land, snow/ice, allowing assessment of the performance of different ERBE ADMs. Finally, the unique characteristics of polar clouds and geotypes entails the evaluation of ERBE ADMs that were designed for global application.

Section 2 discusses issues related to the angular correction for shortwave radiation measurements. The data and methodology used in this study are introduced in Section 3. Section 4 examines the dependency of ERBE flux on viewing geometry. A method for correcting ERBE ADM is proposed in Section 5. Section 6 summarizes the study.

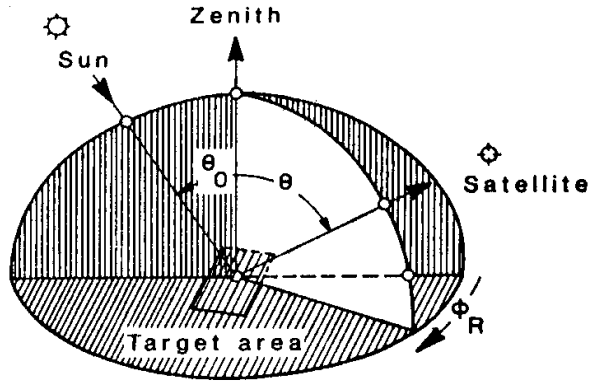

Fig. 1. Satellite, sun and target geometry. θ_0, θ and φ denote solar zenith angle, viewing zenith angle and relative azimuth angle, respectively (from Suttles et al., 1988)

2. Issues on the Angular Correction

2.1 Angular Dependence Model (ADM)

ADM is defined as the ratio of the radiance reflected in a specific direction and the mean radiance reflected in all directions over the upper hemispheric domain. It is generally a scene dependent function of the geometry of illumination and reflection described by three angles, namely, solar zenith angle, viewing zenith angle and relative azimuth angle (see Fig. 1). ADM is thus also referred to as bidirectional reflectance distribution function (BRDF). In addition to scene type, ADM is also a function of wavelength and spatial resolution (Pinty and Verstraete, 1992; Kriebel, 1978). ADMs for narrowband measurements from weather satellites (NOAA and GOES) and resource satellites (LANDSAT and SPOT) differ from those for broadband measurements from experimental space programs (NIMBUS and ERBE) due to their spectral and spatial differences. Recent reviews on the development of narrowband ADMs at the TOA and the surface can be found in Pinty and Verstraete (1992) and Wu et al. (1995).

ADMs have been derived following both empirical and theoretical approaches. Although empirical development of ADMs began with the advent of measurements from early satellite missions such as TIROS-VI (Ruff et al., 1968), TIROS-VII (Arking and Levine, 1967), and NIMBUS-3 (Raschke et al., 1973), it was not until the launch of NIMBUS-7 that acquisition of more complete sets of ADMs was made possible. The ERB instrument aboard the NIMBUS-7 has the

capability of multi-axes scanning to allow radiation measurements from different angles over the same targets (Jacobowitz et al., 1984). Analyses of these data led to both simple parameterized ADMs for clouds (Staylor, 1985), deserts (Staylor and Suttles, 1986), land (Pinty and Raymond, 1986), and more detailed tabulated ADMs for all the major scene types including water, land, snow and cloud (Taylor and Stowe, 1984). Arking and Vemury (1984) assessed the performance of the tabulated model by comparing wide and narrow field of view (FOV) measurements. A large bias error was found in albedo which was attributed to the angular correction. Consequently, they proposed to compute albedo by sorting radiance measurements into different angular bins and then integrating them over all the bins. The method was thus referred to as sorting-angular-bins (SAB), which requires no ADMs but multiple viewing angle measurements. Apart from empirical studies using observational data, many theoretical simulations were conducted for the development of ADMs and evaluation of the angular effects of the atmosphere, cloud and surface (Davies, 1984; Koepke and Kriebel, 1987; Coakley and Kobayashi, 1989). Stuhlmann et al. (1985) compared the NIMBUS-7 ADMs with their modeled ADMs for clouds. The two types of ADMs agree well for low solar zenith angles and poorly for solar zenith angles larger than 70°. Their study also showed that GOES data can be used to complement NIMBUS-7 for cases in which there were no data available from NIMBUS-7.

As a result, a new set of ADMs was developed for applications in ERBE using data primarily from NIMBUS-7, partly from GOES, and occasionally from model simulations (Suttles et al., 1988). The ADMs were developed for 12 scene types listed in Table 1 that include the geotypes of ocean, land, desert, snow, land-ocean mix, for four cloud amounts, namely, clear, partly cloudy, mostly cloudy, and overcast. Prior to the ERBE, the ADMs were developed only for clear and overcast. Note that the ADM for partly clouds is not a simple linear combination of those for clear and overcast skies weighted by cloud amount, since the directional properties of cloud reflection depend strongly on cloud geometry (Coakley and Davies, 1986; Kobayashi, 1993; Barker, 1994).

While ERBE ADMs are the most comprehensive and complete bidirectional models available, they suffer the following major shortcomings. First, ADMs derived from measurements made by polar orbiting platforms tend to factor the latitudinal dependence of reflectivity into a solar zenith angle effect due to a latitudinal variation in scene condition. This was illustrated by Cess and Vulis (1989) over deserts and by Vulis and Cess (1989) over vegetated lands. Second, ADMs developed from NIMBUS-7 data are, in principle, not totally applicable to ERBE data, since their FOVs are different. At nadir, the FOV of NIMBUS-7 is about twice that of ERBE, while at large viewing angles the former is smaller than the latter. A NIMBUS-7 scanning radiometer has an approximately constant FOV, while the FOV of the ERBE scanner increases from nadir to limb. ADM depends on spatial resolution, large FOV tending to average out the natural spatial variation and thereby weakening the anisotropic pattern. The theoretical study by Pinker and Stowe (1990) suggested that TOA bidirectional properties over land surfaces are modified primarily by the atmosphere for the spatial resolution of the NIMBUS-7 ERB. Therefore, it may be adequate to use a single ADM for all types of land. This is, however, definitely not the case for high resolution data from the Advanced Very High Resolution Radiometer (AVHRR) for which the ADM depends on land cover type and greenness of vegetation (Wu et al., 1995). Quantitative studies are lacking as to how many ADMs are appropriate for processing ERBE measurements over land. Third, there is only one overcast model that is applied to all geotypes. Different angular prop-

Table 1. *ERBE Scene Types for Angular Dependence Models*

Number	Scene	Cloud Cover (%)
1	Clear over ocean	0–5
2	Clear over land	0–5
3	Clear over snow	0–5
4	Clear over desert	0–5
5	Clear over land-ocean mix	0–5
6	Partly cloudy over ocean	5–50
7	Partly cloudy over land or desert	5–50
8	Partly cloudy over land-ocean mix	5–50
9	Mostly cloudy over ocean	50–95
10	Mostly cloudy over land or desert	50–95
11	Mostly cloudy over land-ocean mix	50–95
12	Overcast	95–100

erties are expected for overcast over different surface types, unless cloud optical depth is thick enough. The ERBE overcast ADM is more representative of marine overcast conditions, as the samples used in the development of the overcast ADM were taken predominantly over oceans (Suttles et al., 1988). This may pose a serious problem in the Arctic where relatively thin clouds are frequently present over land, snow or ice surfaces. Li and Leighton (1991) found that polar clouds are often so thin that the spectral signature of the underlying surface is discernible at the TOA. Therefore, it is envisaged that the bidirectional characteristics of the surfaces exert an impact on the TOA ADM which undermines the applicability of the ERBE overcast ADM. Evaluating the performance of the ERBE ADMs over polar regions is thus especially needed.

2.2 Scene Identification

It is clear from the above discussions that successful angular correction relies on both correct ADMs and correct scene identification. ERBE scene identification has two aspects: specifying geotype and detecting cloud cover. Geotype is determined a priori according to location and data, while cloud cover is identified dynamically by a maximum-likelihood estimation (MLE) method (Wielicki and Green, 1989). Diekmann and Smith (1989) evaluated the uncertainties in the ERBE fluxes resulting from erroneous cloud identification by the MLE using cloud data obtained from their AVHRR-based algorithm. They found that cloud amounts for thin and low clouds over oceans were underestimated substantially due to the fact that the training data used in the development of the ERBE MLE are averages of all clouds with different heights and thickness. Relative error incurred in TOA shortwave flux may reach as high as 14%. According to Ye (1993), errors in scene identification by the MLE depend also on pixel size. Clear and overcast scenes determined by the MLE near nadir were found to be more likely contaminated, i.e. cloud cover is neither zero nor unity, in comparison to large viewing zenith angles. The dependence of the ERBE scene identification error on viewing zenith angle was also found by Brooks and Fenn (1988a, b) using along-track ERBE scanning data over a short period. Because such a dependency could be misinterpreted as errors in ADMs, correct scene identification is an essential prerequisite for assessing an ADM. The MLE method was also tested by Suttles et al. (1992) who applied the method to broadband NIMBUS-7 ERB data and compared the resulting cloud amounts with those determined from higher spatial and temporal resolution NIMBUS-7 THIR and TOMS data. The agreement is generally within 0.1 over most areas except polar regions where discrepancies reach 0.3. This is attributed to the implicit assumption behind the MLE that cloudy scenes are brighter and colder than clear scenes. This assumption does not often hold in polar areas where clear/cloud contrast is dim in both shortwave and longwave channels. A new scene identification algorithm was developed by Li and Leighton (1991) and Sakellariou et al. (1993) that took advantage of the multi-channel narrowband measurements offered by AVHRR. The cloud amounts deduced from AVHRR and from ERBE differ considerably in the Arctic (Li and Leighton, 1991). Although the AVHRR-based scene identification is not free from errors, it is certainly more reliable than the ERBE technique. Furthermore, polar geotypes prescribed by the ERBE are also erroneous due to the dynamic nature of snow/ice coverage in summer. The algorithm of Li and Leighton (1991) is able to identify both cloud amount and surface types including ocean, land and snow/ice. As such, this study replaces the ERBE scenes by the AVHRR scenes in order to gain an insight into the performance of the ERBE ADM over polar regions.

3. Data and Methodology

The data used in this study consist of both ERBE and AVHRR measurements made from NOAA 9 in the region north of 60 °N during four days throughout the month of July 1985. NOAA 9 was in a sun-synchronic orbit that circulated around the globe about 14 times per day. The number of daytime pass over a fixed target increases from 7 at 60° to 14 at the pole. Both ERBE and AVHRR radiometers scan the Earth in a cross-track direction, allowing simultaneous and coincident observations at varying spatial resolutions. The two types of data were combined by matching 8×8 AVHRR global area coverage (GAC) pixels of 4-km resolution to one ERBE

Table 2. *Angular bins Used by ERBE ADMs (Degrees)*

No.	Solar zenith	No.	Viewing zenith	No.	Relative azimuth
1	0–25.84	1	0–15	1	0–9
2	25.84–36.87	2	15–27	2	9–30
3	36.87–45.57	3	27–39	3	30–60
4	45.57–53.13	4	39–51	4	60–90
5	53.13–60.00	5	51–63	5	90–120
6	60.00–66.42	6	63–75	6	120–150
7	66.42–72.54	7	75–90	7	150–171
8	72.54–78.46			8	171–180
9	78.46–84.26				
10	84.26–90.00				

pixel. The scene with respect to both cloud cover and surface type for an ERBE pixel was determined by the scenes of the 64 AVHRR pixels collocated to the ERBE pixel (Li and Leighton, 1991). Based on this new scene type, an appropriate ERBE ADM was applied to the ERBE radiance measurement to compute a new flux which is then converted into an albedo. Tri-linear interpolation in terms of solar zenith angle, viewing zenith angle and relative azimuth angle was carried out when the ERBE ADM was implemented, since the ERBE anisotropic factors were averaged over discrete angular bins of considerable ranges listed in Table 2.

A simple way to test the validity of an ADM is to see if the derived albedo changes with viewing zenith angle and relative azimuth angle. If an ADM is perfect, the resulting albedo should be independent of viewing geometry, provided that the scene is stable and identified correctly. To this end, all data were first sorted into the angular bins listed in Table 2. As in the development of ERBE ADMs, the dependence of reflection on relative azimuth angle is assumed to be symmetric with respect to the principal plane determined by the sun, satellite and target (see Fig. 1). Owing to the limited number of measurements, the data are classified according to scene type regardless of geographic location. The cross-track scanning mode and convergence of orbits in the polar region render little bias in the sample population with respect to viewing zenith angle bin. However, the measurements are restricted to certain relative azimuth angle bins, mainly bin 3, 4, and 6, owing to the characteristics of sun-synchronous orbits. Furthermore, different scenes are sampled unequally, since the degree of overlapping changes with latitude that is further correlated with scene type. The minimum sample population required for a reliable estimate of a bin-mean albedo depends on the variability of the scene. Pure scenes including uniform geotypes under clear and overcast conditions turn out to have large populations and small variability, which permits an analysis of the angular variation of the derived albedo. Mixed scenes including partly and mostly clouds and mixed geotypes have too few measurements in a bin to derive a representative albedo, or too many blank bins. Assessment of the ADMs for these scene types is thus handicapped. On the other hand, however, evaluation of the ADMs for pure ocean and land sheds light on the ADMs for ocean-land mix, since the latter were derived from the ADMs for the former. Failure to evaluate the ADMs for partly and mostly cloudy conditions does not pose a serious problem for radiation budget studies in the Arctic, where overcast clouds occur much more frequently than broken clouds during summer.

4. Results

After sorting the data, the mean albedos and their standard deviations over pure scenes are computed for all the bins in which there are multiple measurements. The standard deviation of a mean albedo serves as an indication of the statistical uncertainty resulting from insufficient sampling and variability of the scene. The mean albedos are plotted as functions of viewing zenith angle for different ranges of relative azimuth angle and solar zenith angle (see Figs. 2–5). For the sake of

clarity, variations with respect to relative azimuth angle are shown in three coarse intervals instead of eight used by the ERBE. Their ranges are 0–60, 60–120 and 120–180, representing approximately reflection in forward, sideward and backward directions, respectively. Discrepancies between the curves reveal to what extent an ERBE ADM inadequately accounts for the variation of reflectance with relative azimuth angle, while the variation of albedo with viewing zenith angle indicates the deficiency for an ERBE ADM to represent the dependence on viewing zenith angle. In view of the statistical uncertainty, a variation is considered to be meaningful only when it is significantly larger than the standard deviation.

Figure 2 shows the results obtained over clear oceans. Moderate increases of albedo with viewing zenith angle are noted when the cosine of the solar zenith angle is smaller than 0.3. As the cosine of the solar zenith angle increases, the variation of albedo with viewing zenith angle gradually becomes less pronounced. The differences in albedo due to relative azimuth angle are essentially within the ranges of uncertainty. It follows from Fig. 3 that the ERBE ADM for clear land does a good job of accounting for the angular dependence on viewing zenith angle, illustrated by the flat lines. There are small but systematic discrepancies among different intervals of relative azimuth angle. Overall, the performance of the clear-land ADM is superior to the clear-ocean ADM, probably because ocean shows much stronger anisotropic reflectance and is thus more sensitive to angular correction than is land. However, this is not the case for clear snow/ice, whose reflectance shows even less variation with viewing geometry (Taylor and Stowe, 1984). Despite the large uncertainties in Fig. 4 arising from a variety of snow/ice conditions in the summer Arctic, it appears that the snow/ice albedos change substantially with both viewing zenith angle and relative azimuth angle. The poor performance of the snow/ice ADM in the summer Arctic may be attributed to the fact that the measurements used in the establishment of the clear-snow/ice ERBE ADM were more representative of winter snow that is much fresher and brighter than the old snow or ice present in the summer Arctic. Since specular reflection augments with snow age, reflectance becomes more anisotropic toward mid summer (July) after many freezing/thawing events (Dirmhirn and Eaton, 1975). Moreover, snow accumulation on sea ice may vanish after thawing in early summer and thus much of the data shown in Fig. 4 represents sea ice more than snow. Sea ice has larger grain sizes than snow and thereby tends to reflect more anisotropically (Steffen, 1987). Furthermore, specular reflection increases with solar zenith angle (Salomonson and Marlatt, 1968). That may explain the stronger viewing zenith angle dependence in Fig. 4a to 4d compared to Fig. 4e and 4f. As for overcast, only overcast-over-snow/ice is shown (Figure 5).There are insufficient data to evaluate the performance of the ADMs for overcast scenes over other surface types. As was conjectured earlier, the ERBE overcast ADM leads to large errors when it is applied to overcast-over-snow/ice scene. This is seen from the large and well behaved variations of albedo with both viewing zenith angle and relative azimuth angle. The statistical uncertainties shown in Fig. 5 are very small compared to the angular variations of albedo owing to the larger number of samples. Albedo decreases with viewing zenith angle when the cosine of the solar zenith angle is smaller than 0.5 at a rate dependent strongly on relative azimuth angle, quicker in the sideward direction than in other directions. As the cosine of the solar zenith angle increases, the performance of ERBE ADM improves significantly. This appears to be a rather universal phenomenon as it is observed for all the cases examined here.

It follows from Figs. 2–5 that most of the albedos derived from the ERBE ADMs are subject to variation with viewing geometry. The magnitude of variation depends on scene type and solar zenith angle. Owing to the small number of samples, it is not feasible to use the present data set to generate a new set of ADMs for use in the Arctic. As a result, qualitative assessment of the performance of the ERBE ADMs is the main objective of this study. Nevertheless, an attempt is made to correct the ERBE ADM for the overcast-over-snow/ice scene for which the statistical uncertainties are small and the dependence of albedo on viewing zenith angle is well defined. The correction is done by redefining the values of ADM for those bins that contain many enough samples. Due to the limitation of the data, the exercise is intended more for illustration of a methodology than for provision of an revised model.

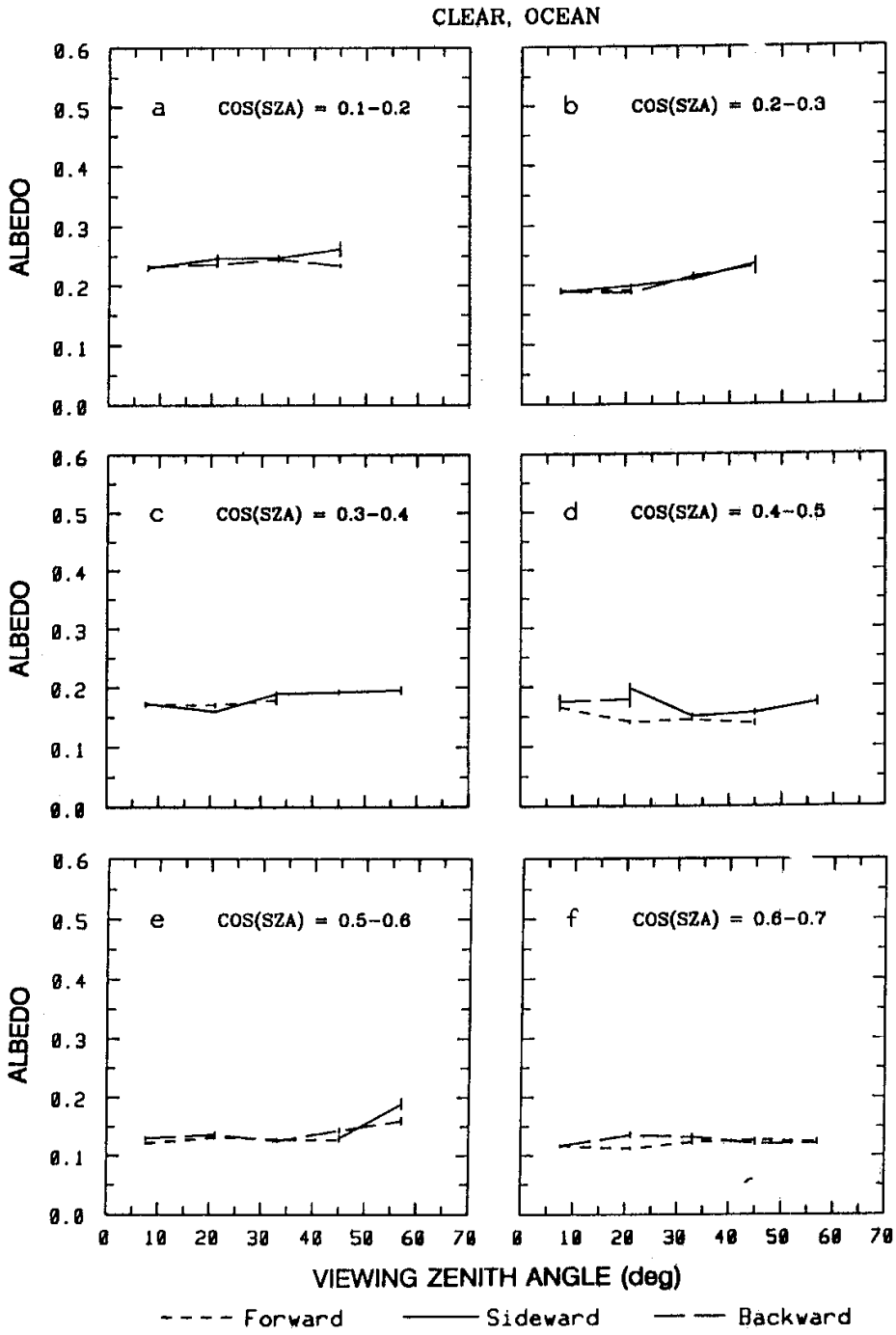

Fig. 2. Variations of bin-mean albedo with viewing zenith angle for different ranges of relative azimuth angle and solar zenith angle over clear-sky ocean. Forward, sideward and backward directions have relative azimuth angles of 0°–60°, 60°–120° and 120°–180°, respectively

5. Normalization of an ADM

An ADM is defined by:

$$R(\theta_0, \theta, \phi) = \frac{\pi L(\theta_0, \theta, \phi)}{M(\theta_0)} \tag{1}$$

where L denotes reflected radiance; M reflected flux. θ_0, θ and ϕ represent solar zenith angle, viewing zenith angle and relative azimuth angle, respectively. Thus, if the reflected radiance is isotropic (Lambertian), $R = 1$. Flux and radiance are related by

$$M(\theta_0) = \int_0^{2\pi} d\phi \int_0^{\pi/2} L(\theta_0, \theta, \phi) \cos\theta \sin\theta \, d\theta \tag{2}$$

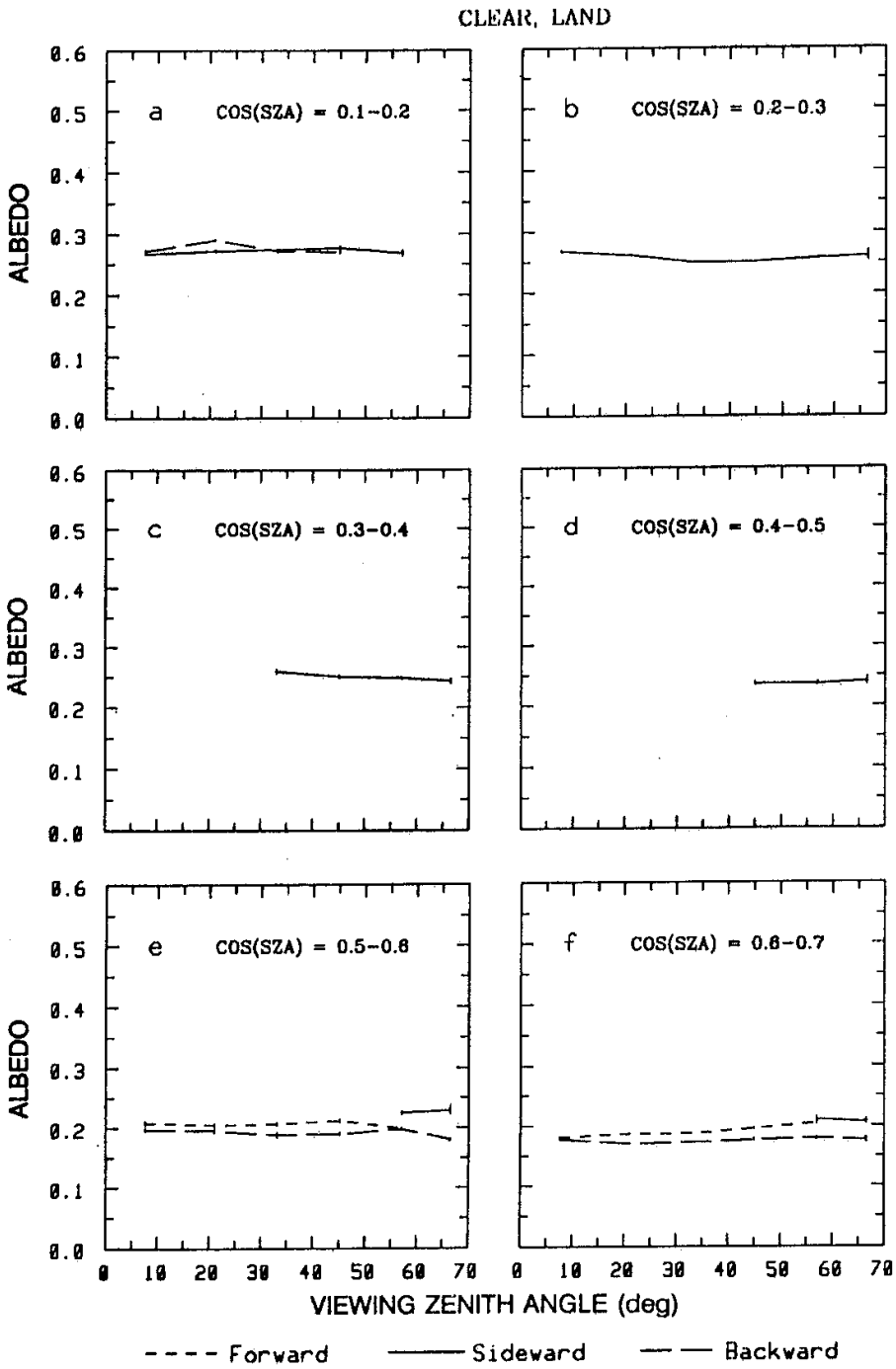

Fig. 3. Same as Fig. 2 but for clear-sky land

Reflectance and albedo are defined respectively as

$$a(\theta_0, \theta, \phi) = \frac{\pi L(\theta_0, \theta, \phi)}{F(\theta_0)} \tag{3}$$

$$A(\theta_0) = \frac{M(\theta_0)}{F(\theta_0)} \tag{4}$$

where $F(\theta_0)$ is the solar flux incident at the top of the atmosphere, Using (3) and (4), (1) can be rewritten as

$$R(\theta_0, \theta, \phi) = \frac{a(\theta_0, \theta, \phi)}{A(\theta_0)} \tag{5}$$

It follows from (5) that the determination of an ADM requires knowledge of reflectance and albedo. Reflectance data are available for some viewing bins in which there are sufficient samples to derive reliable bin-mean values. These bins are

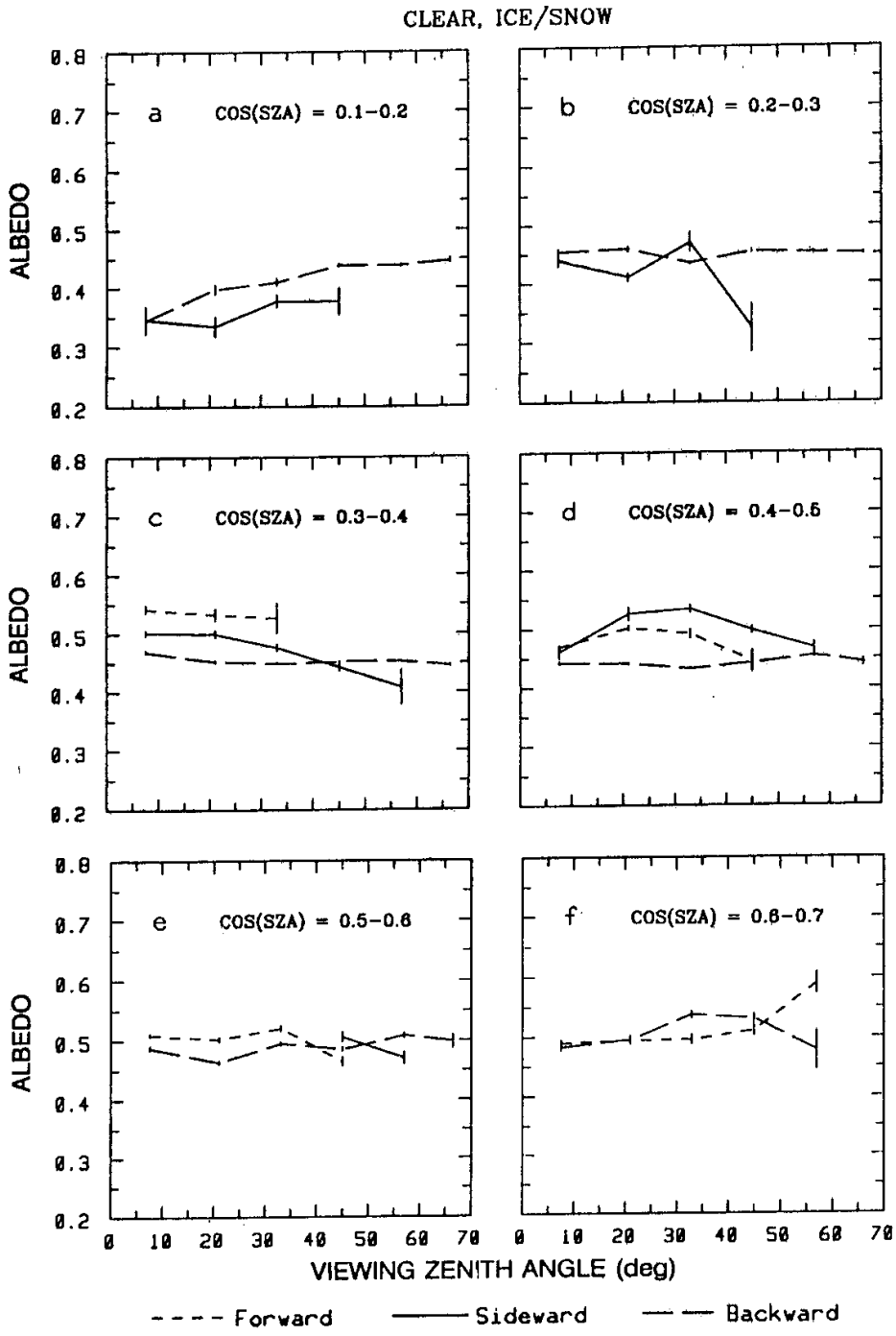

Fig. 4. Same as Fig. 2 but for clear-sky snow/ice

simply referred to as valid bins. The validity of a bin is determined by the ratio of the standard deviation of reflectance to the mean reflectance. When this ratio is smaller than one percent, the bin is considered to be valid and the data in that bin are used. This is a rigid criterion which excludes most bins containing scenes other than over-cast-over-snow/ice to assure that the statistical uncertainty of the corrected ADM is small. For over-cast-over-snow/ice, there are about 14 bins that satisfy the criterion with a mean sample of about 1500 per bin.

Value of $A(\theta_0)$ in (5) is unknown. Those derived from the ERBE ADM may be unreliable unless they are invariant with viewing geometry. Therefore, the albedo used to correct an ADM is obtained directly from the integration of reflectance. From (2) through (4), albedo is

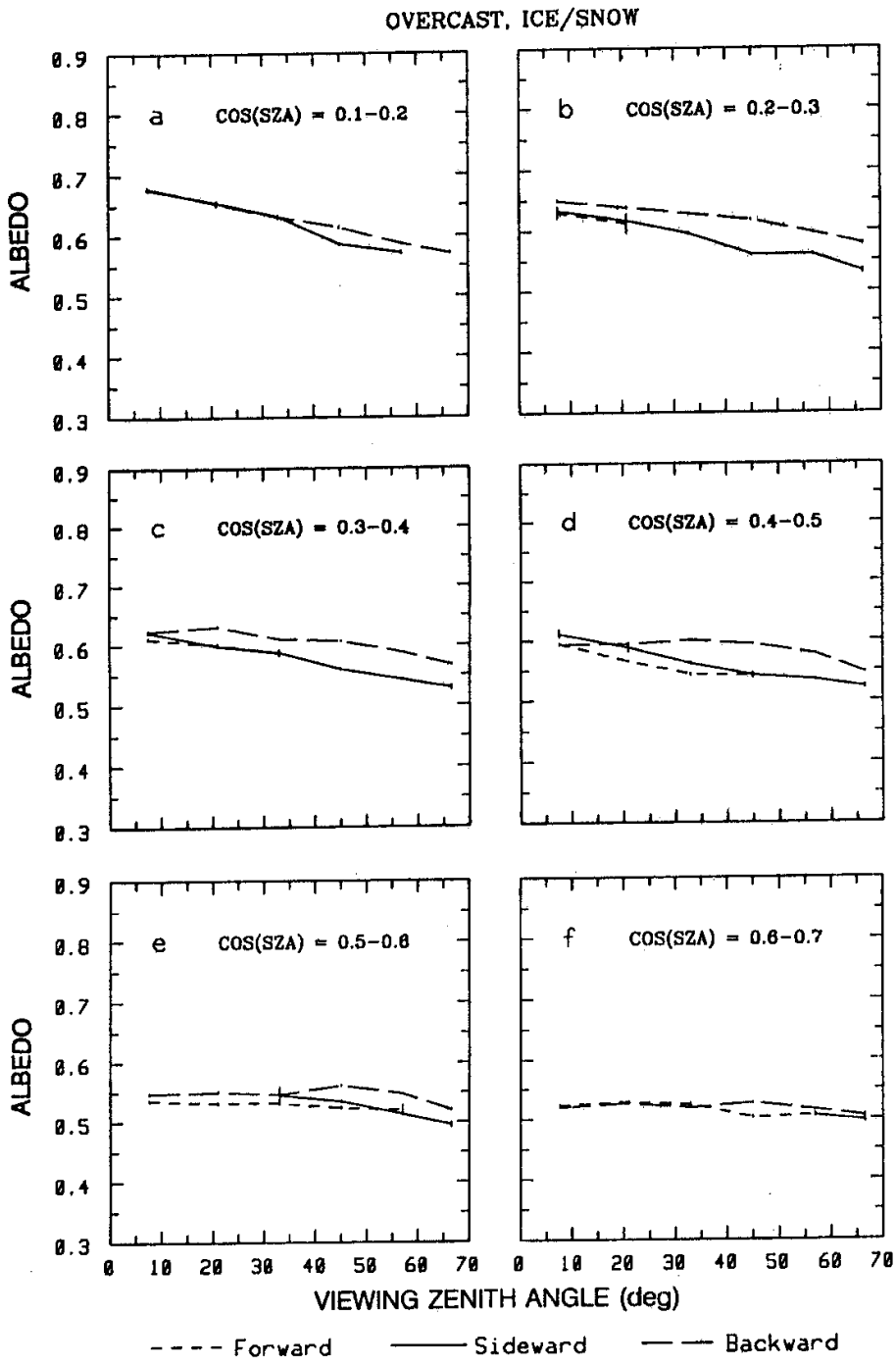

Fig. 5. Same as Fig. 2 but for overcast-over-snow/ice

expressed as

$$A(\theta_0) = \frac{1}{\pi}\int_0^{2\pi}\int_0^{\pi/2} a(\theta_0,\theta,\phi)\cos\theta\sin\theta\, d\theta\, d\phi$$
$$= \frac{1}{\pi}\iint_{(\alpha)} a(\theta_0,\theta,\phi)\cos\theta\sin\theta\, d\theta\, d\phi \qquad (6)$$
$$+\frac{1}{\pi}\iint_{(\beta)} A(\theta_0)R(\theta_0,\theta,\phi)\cos\theta\sin\theta\, d\theta\, d\phi$$

where α denotes the viewing domain composed of valid bins, and β the remaining domain. In the remaining domain, $R(\theta_0,\theta,\phi)$ is derived from ERBE ADM. It follows from (6) that

$$A(\theta_0) = \frac{\frac{1}{\pi}\iint_{(\alpha)} a(\theta_0,\theta,\phi)\cos\theta\sin\theta\, d\theta\, d\phi}{1-\frac{1}{\pi}\iint_{(\beta)} R(\theta_0,\theta,\phi)\cos\theta\sin\theta\, d\theta\, d\phi} \qquad (7)$$

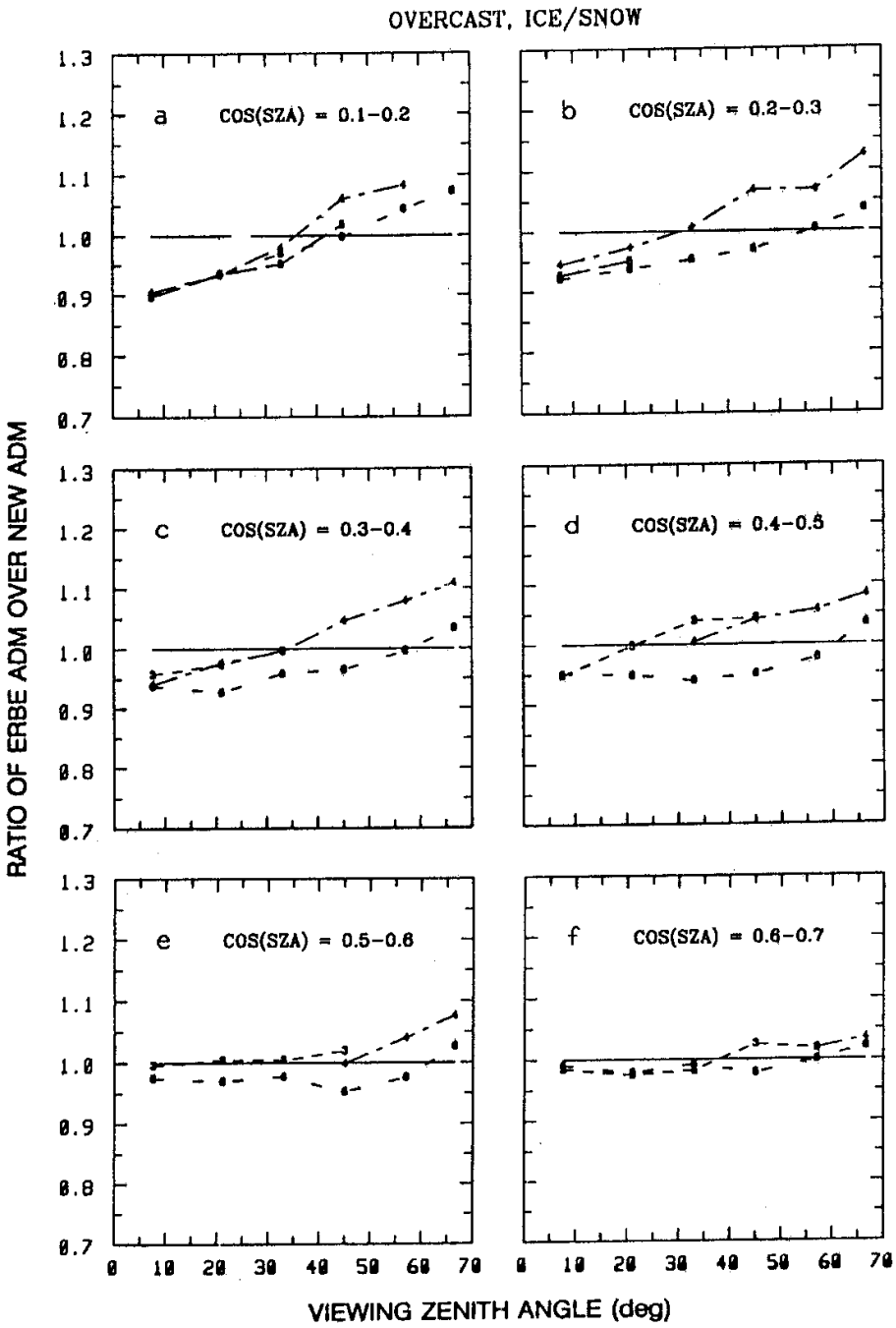

Fig. 6. The ratios of the anisotropic factors from the ERBE ADMs over those from the corrected ERBE ADMs. The numbers on the curves denote the azimuth bins whose ranges defined in Table 2

The corrected ADM is, therefore, given by the following conditional function:

$$R'(\theta_0,\theta,\phi)=\begin{cases}\dfrac{a(\theta_0,\theta,\phi)}{A(\theta_0)} & \theta,\phi\in\alpha\\ R(\theta_0,\theta,\phi) & \theta,\phi\in\beta\end{cases} \tag{8}$$

where $R(\theta_0,\theta,\phi)$ is the ERBE ADM, $a(\theta_0,\theta,\phi)$ and $A(\theta_0)$ are given by (3) and (7), respectively. It can be shown that the ADM defined by (8) satisfies the normalization constraint, i.e.,

$$\frac{1}{\pi}\int_0^{2\pi}\int_0^{\pi/2} R'(\theta_0,\theta,\phi)\cos\theta\sin\theta\,d\theta\,d\phi=1 \tag{9}$$

Note that an ADM can only be corrected over the valid domain. Outside this domain, lack of measurements prohibits redefining the ADM. On the other hand, bins with few or no samples represent the viewing geometries from which

a scanner aboard a polar orbiting satellite seldom measures and thus angular correction is of less significance. The corrected ADM will lead to an invariant albedo $A(\theta_0)$ for viewing angles falling within the valid domain.

Numerical integration of (7) was conducted for overcast-over-snow/ice scenes using the ERBE angular discretion delineated in Table 2. After the albedo was obtained, it was used together with bin-mean reflectance data to determine R' over the valid domain. Figure 6 shows the ratio of R/R' between original and new ADM. In many cases, they differ by more than ten percent. Relative to the corrected ADM, the ERBE ADM tends to underestimate the anisotropic factor at small viewing zenith angles and overestimate it at large viewing zenith angles. Underestimation is more prevalent for the relative azimuth angles in bin 6, whereas the reverse is the case for bins 3 and 4.

6. Summary

Since the Earth Radiation Budget Experiment (ERBE) provides high quality radiative flux measurements of the earth-atmosphere system, ERBE data have been widely used for a variety of climate studies. It should be borne in mind, however, that many inversion algorithms were employed in the processing of ERBE data, and they are potential sources of uncertainty. The most error-prone processing arises from angular correction that is needed for obtaining fluxes from radiances. While many investigators have assessed the performance of ERBE angular dependence model (ADM), most have focused on low latitude oceans. This study evaluated the performance of the ERBE ADM over the Arctic. Four potential problems may degrade its performance in the Arctic summer: mis-identification of scene type; correlation between the properties of scene and latitude; disparity in spatial resolution between the ERBE and Nimbus 7 radiometers; and differences in scene characteristics for the development and for the application of ADMs. Overlapping of polar orbits in the Arctic permits assessment of ERBE ADMs.

Due to problems with ERBE scene identification, ERBE scene types were replaced by those deduced from AVHRR measurements that were matched to ERBE observations. The ERBE ADMs selected according to the AVHRR scenes were used to derive TOA albedos from radiances. The albedo data were first sorted into angular bins and bin mean values were then plotted against viewing zenith angle for different ranges of relative azimuth angle and solar zenith angle. If an ADM is perfect, the inferred albedo is independent of viewing geometry. According to the variations of albedo with viewing geometry, ERBE ADMs were found to perform best over land, worst over snow/ice in the Arctic summer, and moderately over water except at large solar zenith angles. The overcast ERBE ADM is inadequate in the Arctic where clouds are generally thinner than the global mean. A methodology for correcting ERBE ADMs was proposed that normalizes the anisotropic factor over the bins containing sufficient measurements. The correction is feasible for an overcast-over-snow/ice scene for which there are a large number of samples. The corrected ADM renders albedo independent of viewing geometry and satisfies the normalization condition.

Acknowledgments

The author is indebted to Prof. H. G. Leighton for helpful discussions during the course of the study.

References

Arking, A., 1991: The radiative effects of clouds and their impact on climate. *AMS Bulletin*, **72**, 795–813.

Arking, A., Vemury, S., 1984: The NIMBUS 7 ERB data set: A critical analysis. *J. Geophys. Res.*, **89**, 5089–5097.

Arking, A., Levine, J. S., 1967: Earth albedo measurements, July 1963 to June 1964. *J. Atmos. Sci.*, **24**, 721–724.

Baldwin, D. G., Coakley, Jr., J. A., 1991: Consistency of earth radiation budget experiment bidirectional models and the observed anisotropy of reflected sunlight. *J. Geophys. Res.*, **96**, 5195–5207.

Barker, H. W., Li, Z., Blanchet, J.-P., 1994: Radiative characteristics of the Canadian Climate Centre second-generation general circulation model. *J. Climate*, **7**, 1070–1091.

Barker, H. W., Li, Z., 1995: Improved simulation of shortwave radiative transfer in the CCC GCM. *J. Climate*, **8**, 2213–2223.

Barker, H. W., 1994: Solar radiative transfer for wind-sheared cumulus cloud fields. *J. Atmos. Sci.*, **51**, 1141–1156.

Barkstrom, B. R., Smith, G. L., 1986: The earth radiation budget experiment: science and implementation. *Rev. Geophys.*, **24**, 379–390.

Brooks, D. R., Fenn, M. A., 1988a: Summary of along-track data from the earth radiation budget satellite for several representative ocean regions. *NASA Ref. Pub.*, **1197**, 214 pp.

Brooks, D. R., Fenn, M. A., 1988b: Summary of along-track data from the earth radiation budget satellite for several major desert regions. *NASA Ref. Pub.*, **1206**, 145 pp.

Cess, R. D., Potter, G. L., Gates, W. L., Morcrette, J.-J., Corsetti, L., 1992: Comparison of general circulation models to earth radiation budget experiment data: computation of clear-sky fluxes. *J. Geophys. Res.*, **97**, 20421–20426.

Cess, R. D., Vulis, I. L., 1989: Intercomparison and interpretation of satellite-derived directional albedos over deserts. *J. Climate*, **2**, 393–407.

Coakley, J. A., Jr., Davies, R., 1986: The effects of cloud sides on reflected solar radiation as deduced from satellite observations. *J. Atmos. Sci.*, **43**, 1025–1035.

Coakley, J. A., Jr., Kobayashi, T., 1989: Broken cloud biases in albedo and surface insolation derived from imagery data. *J. Climate*, **2**, 721–730.

Davies, R., 1984: Reflected solar radiances from broken cloud scenes and the interpretation of scanner measurements. *J. Geophys. Res.*, **89**, 1259–1266.

Diekmann, F. J., Smith, G. L., 1989: Investigation of scene identification algorithms for radiation budget measurements. *J. Geophys. Res.*, **94**, 3395–3412.

Dirmhirn, I., Eaton, F. D., 1975: Some characteristics of the albedo of snow. *J. Appl. Meteor.*, **14**, 375–379.

Dlhopolsky, R., Cess, R. D., 1993: Improved angular directional models for clear-sky ocean derived from Earth Radiation Budget Satellite shortwave radiances. *J. Geophys. Res.*, **98**, 16,713–16,721.

Harrison, E. F., Minnis, P., Barkstrom, B. R., Ramanathan, V., Cess, R. D., Gibson, G. G., 1990: Seasonal variation of cloud radiative forcing derived from the earth radiation budget experiment. *J. Geophys. Res.*, **95**, 18687–18703.

Jacobowitz, H., Soule, H. V., Kyle, H. L., House, Frederick B., the NIMBUS 7 ERB Experiment Team, 1984: The earth radiation budget (ERB) experiment: An overview. *J. Geophys. Res.*, **89**, 5021–5038.

Kiehl, J. T., Ramanathan, V., 1990: Comparison of cloud forcing derived from the earth radiation budget experiment with that simulated by the NCAR community climate model. *J. Geophys. Res.*, **95**, 11679–11698.

Kobayashi, T., 1993: Effects due to cloud geometry on biases in the albedo derived from radiance measurements. *J. Climate*, **6**, 120–128.

Koepke, P., Kriebel, K. T., 1987: Improvements in the shortwave cloud-free radiation budget accuracy, Part I: Numerical study including surface anisotropy. *J. Climate Appl. Meteor.*, **26**, 374–395.

Li, Z., Leighton, H. G., 1991: Scene identification and its effect on cloud radiative forcing in the Arctic. *J. Geophys. Res.*, **96**, 9175–9188.

Li, Z., Leighton, H. G., 1993: Global climatology of solar radiation budgets at the surface and in the atmosphere from 5 years of ERBE data. *J. Geophys. Res.*, **98**, 4919–4930.

Li, Z., Whitlock, C., Charlock, T., 1995: Assessment of the global monthly mean surface insolation estimated from satellite measurements using the Global Energy Balance Archive data. *J. Climate*, **8**, 315–328.

Pinker, R. T., Stowe, L. L., 1990: Modelling planetary bidirectional reflectance over land. *Int. J. Remote Sensing*, **11**, 113–123.

Pinty, B., Verstraete, M. M., 1992: On the design and validation of surface bidirectional reflectance and albedo models. *Remote Sensing Environ.*, **41**, 155–167.

Pinty, B., Ramond, D., 1986: A simple bidirectional reflectance model for terrestrial surfaces. *J. Geophys. Res.*, **91**, 7803–7808.

Ramanathan, V., Cess, R. D., Harrison, E. F., Minnis, P., Barkstrom, B. R., Ahmad, E., Hartmann, D., 1989: Cloud-radiative forcing and climate: results from the earth radiation budget experiment. *Science*, **243**, 57–63.

Raschke, E., Vonder Haar, T. H., Bandeen, W. R., Pasternak, M., 1973: The annual radiation balance of the earth-atmosphere system during 1969–1970 from Nimbus 3 measurements. *J. Atmos. Sci.*, **30**, 341–364.

Ruff, I., Koffer, R., Fritz, S., Winston, J. S. Rao, P. K., 1968: Angular distribution of solar radiation reflected from clouds as determined from TIROS IV radiometer measurements. *J. Atmos. Sci.*, **25**, 323–332.

Sakellariou, N. K., Leighton, H. G., Li, Z., 1993: Identification of clear and cloudy pixels at high latitudes from AVHRR radiances. *Int. J. Remote Sensing*, **14**, 2005–2024.

Smith, G. L., Green, R. N., Raschke, E., Avis, L. M., Suttles, J. T., Wielicki, B. A., Davies, R., 1986: Inversion methods for satellite studies of the earth's radiation budget: development algorithms for the ERBE mission. *Rev. Geophys.*, **24**, 407–421.

Salomonson, V. V., Marlatt, D. C., 1968: Anisotropic solar reflectance over white sand, snow, and stratus clouds. *J. Appl. Meteor.*, **7**, 475–483.

Staylor, W. F., 1985: Reflection and emission models for clouds derived from Nimbus 7 Earth Radiation Budget scanner measurements. *J. Geophys. Res.*, **90**, 8075–8079.

Staylor, W. F., Suttles, J. T., 1985: Reflection and emission models for deserts derived from Nimbus-7 ERB scanner measurements. *J. Climate Appl. Meteor.*, **25**, 196–202.

Steffen, K., 1987: Bidirectional reflectance of snow. in Large Scale Effects of Snowcover, *Proc. IAHS Symp.*, 19–22 August 1987, Vancouver, Canada, 415–425.

Stuhlmann, R., Raschke, E., 1987: Satellite measurements of the earth radiation budget: sampling and retrieval of short wave exitances – a sampling study. *Beitr. Phys. Atmos.*, **60**, 393–410.

Stuhlmann, R., Minnis, P., Smith, G. L., 1985: Cloud bidirectional reflectance functions: A comparison of experimental and theoretical results. *Appl. Opt.*, **24**, 396–401.

Suttles, J. T., Wielicki, B. A., Vemury, S., 1992: Top-of-atmosphere radiation fluxes: validation of ERBE scanner inversion algorithm using NIMBUS-7 ERB data. *J. Appl. Meteor.*, **31**, 784–796.

Suttles, J. T., Green, R. N., Minnis, P., Smith, G. L., Staylor, W. F., Wielicki, B. A., Walker, I. J., Young, D. F., Taylor, V. R., Stowe, L. L., 1988: Angular radiation models for Earth-atmosphere system. Vol. 1-Shortwave radiation. *NASA Refer. Publ.*, **1184**, 114 pp.

Vulis, I. L., Cess, R. D., 1989: Interpretation of surface and planetary directional albedos for vegetated regions. *J. Climate*, **2**, 974–985.

Taylor, V. R., Stowe, L. L., 1984: Reflectance characteristics of uniform earth and cloud surfaces derived from Nimbus-7 ERB. *J. Geophys. Res.*, **89**, 4987–4996.

Wielicki, B. A., Green, R. N., 1989: Cloud identification for ERBE radiative flux retrieval. *J. Appl. Meteor.*, **28**, 1133–1146.

Wu, A., Li, Z., Cihlar, J., 1995: The effects of land cover type, greenness and sun angle on the bidirectional distributions of AVHRR reflectances. *J. Geophys. Res.*, **100**, 9179–9192.

Ye, Q., 1993: The space-scale dependence of the observed anisotropy of reflected and emitted radiation, Ph.D. Dissertation, Oregon State University, pp 159.

Authors' address: Dr. Z. Li, Canada Centre for Remote Sensing, 588 Booth Street, Ottawa, Canada K1A 0Y7.